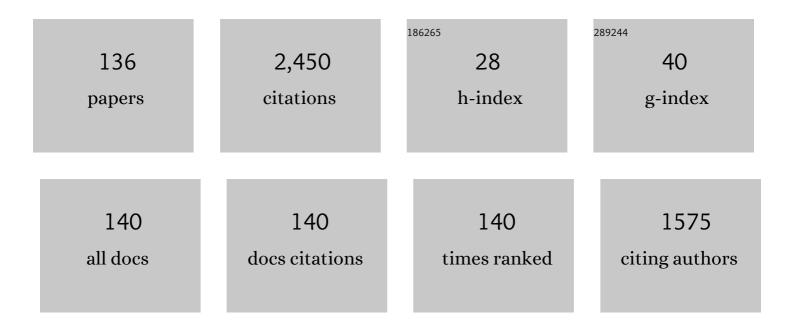


List of Publications by Year in descending order

Source: https://exaly.com/author-pdf/8554352/publications.pdf Version: 2024-02-01



#	Article	IF	CITATIONS
1	Seasonal and quasiâ€biennial variations in the migrating diurnal tide observed by Thermosphere, Ionosphere, Mesosphere, Energetics and Dynamics (TIMED). Journal of Geophysical Research, 2009, 114, .	3.3	117
2	Using TIMED/SABER nightglow observations to investigate hydroxyl emission mechanisms in the mesopause region. Journal of Geophysical Research, 2012, 117, .	3.3	76
3	Global distribution and interannual variations of mesospheric and lower thermospheric neutral wind diurnal tide: 1. Migrating tide. Journal of Geophysical Research, 2008, 113, .	3.3	74
4	Mesopause structure from Thermosphere, Ionosphere, Mesosphere, Energetics, and Dynamics (TIMED)/Sounding of the Atmosphere Using Broadband Emission Radiometry (SABER) observations. Journal of Geophysical Research, 2007, 112, .	3.3	72
5	Thermosphere and ionosphere response to subauroral polarization streams (SAPS): Model simulations. Journal of Geophysical Research, 2012, 117, .	3.3	67
6	Global distribution and interannual variations of mesospheric and lower thermospheric neutral wind diurnal tide: 2. Nonmigrating tide. Journal of Geophysical Research, 2008, 113, .	3.3	53
7	Strong longitudinal variations in the OH nightglow. Geophysical Research Letters, 2010, 37, .	4.0	52
8	Concentric gravity waves over northern China observed by an airglow imager network and satellites. Journal of Geophysical Research D: Atmospheres, 2015, 120, 11,058.	3.3	51
9	Variations of global gravity waves derived from 14Âyears of SABER temperature observations. Journal of Geophysical Research D: Atmospheres, 2017, 122, 6231-6249.	3.3	50
10	A comparison of the effects of CIR―and CME―nduced geomagnetic activity on thermospheric densities and spacecraft orbits: Case studies. Journal of Geophysical Research, 2012, 117, .	3.3	46
11	Ionospheric Day-to-Day Variability Around the Whole Heliosphere Interval in 2008. Solar Physics, 2011, 274, 457-472.	2.5	45
12	Anisotropy of the horizontal velocity fluctuation field in the large wavenumber region. Science in China Series D: Earth Sciences, 2003, 46, 210-216.	0.9	44
13	A comparison of the effects of CIR―and CME―nduced geomagnetic activity on thermospheric densities and spacecraft orbits: Statistical studies. Journal of Geophysical Research: Space Physics, 2014, 119, 7928-7939.	2.4	44
14	The features and a possible mechanism of semiannual variation in the peak electron density of the low latitude F2 layer. Journal of Atmospheric and Solar-Terrestrial Physics, 2003, 65, 47-57.	1.6	42
15	Seasonal and QBO variations in the OH nightglow emission observed by TIMED/SABER. Journal of Geophysical Research, 2010, 115, .	3.3	42
16	Statistical characteristics of gravity wave activities observed by an OH airglow imager at Xinglong, in northern China. Annales Geophysicae, 2011, 29, 1401-1410.	1.6	39
17	Evidence for nonmigrating tides produced by the interaction between tides and stationary planetary waves in the stratosphere and lower mesosphere. Journal of Geophysical Research D: Atmospheres, 2014, 119, 471-489.	3.3	39
18	Perturbations of the sodium layer: controlled by chemistry or dynamics?. Geophysical Research Letters, 2003, 30, .	4.0	36

#	Article	IF	CITATIONS
19	Comparison between the temperature measurements by TIMED/SABER and lidar in the midlatitude. Journal of Geophysical Research, 2006, 111, .	3.3	36
20	Signature of an overturning gravity wave in the mesospheric sodium layer: Comparison of a nonlinear photochemical-dynamical model and lidar observations. Journal of Geophysical Research, 2006, 111, .	3.3	36
21	A numerical study of the effect of gravity-wave propagation on minor species distributions in the mesopause region. Journal of Geophysical Research, 2003, 108, n/a-n/a.	3.3	35
22	Nonlinear interactions between gravity waves with different wavelengths and diurnal tide. Journal of Geophysical Research, 2008, 113, .	3.3	35
23	First observation of mesospheric and thermospheric winds by a Fabry-Perot interferometer in China. Science Bulletin, 2010, 55, 4046-4051.	1.7	34
24	Mesoscale fieldâ€aligned irregularity structures (FAIs) of airglow associated with mediumâ€scale traveling ionospheric disturbances (MSTIDs). Journal of Geophysical Research: Space Physics, 2015, 120, 9839-9858.	2.4	34
25	A statistical analysis of equatorial plasma bubble structures based on an allâ€ s ky airglow imager network in China. Journal of Geophysical Research: Space Physics, 2016, 121, 11,495.	2.4	34
26	An observational and theoretical study of the longitudinal variation in neutral temperature induced by aurora heating in the lower thermosphere. Journal of Geophysical Research: Space Physics, 2013, 118, 7410-7425.	2.4	32
27	Gravity wave variations in the polar stratosphere and mesosphere from SOFIE/AIM temperature observations. Journal of Geophysical Research D: Atmospheres, 2014, 119, 7368-7381.	3.3	31
28	Variations of the nighttime thermospheric mass density at low and middle latitudes. Journal of Geophysical Research, 2010, 115, .	3.3	28
29	FPI observations of nighttime mesospheric and thermospheric winds in China and their comparisons with HWM07. Annales Geophysicae, 2013, 31, 1365-1378.	1.6	28
30	A case study of the mesospheric 6.5â€day wave observed by radar systems. Journal of Geophysical Research, 2008, 113, .	3.3	27
31	The effect of periodic variations of thermospheric density on CHAMP and GRACE orbits. Journal of Geophysical Research, 2011, 116, n/a-n/a.	3.3	27
32	Orographic Primary and Secondary Gravity Waves in the Middle Atmosphere From 16‥ear SABER Observations. Geophysical Research Letters, 2019, 46, 4512-4522.	4.0	27
33	A comparison of mesospheric winds measured by FPI and meteor radar located at 40N. Science China Technological Sciences, 2012, 55, 1245-1250.	4.0	25
34	The longitudinal variation of the daily mean thermospheric mass density. Journal of Geophysical Research: Space Physics, 2013, 118, 515-523.	2.4	25
35	Interesting Equatorial Plasma Bubbles Observed by Allâ€6ky Imagers in the Equatorial Region of China. Journal of Geophysical Research: Space Physics, 2017, 122, 10,596.	2.4	25
36	The effect of â^1⁄427 day solar rotation on ionospheric <i>F</i> ₂ region peak densities (<i>N</i> _{<i>m</i>} <i>F</i> ₂). Journal of Geophysical Research, 2012, 117, .	3.3	24

#	Article	IF	CITATIONS
37	Investigation of a mesospheric bore event over northern China. Annales Geophysicae, 2013, 31, 409-418.	1.6	24
38	Large winds and wind shears caused by the nonlinear interactions between gravity waves and tidal backgrounds in the mesosphere and lower thermosphere. Journal of Geophysical Research: Space Physics, 2014, 119, 7698-7708.	2.4	23
39	Momentum balance and gravity wave forcing in the mesosphere and lower thermosphere. Geophysical Research Letters, 2009, 36, .	4.0	22
40	Responses of the lower thermospheric temperature to the 9 day and 13.5 day oscillations of recurrent geomagnetic activity. Journal of Geophysical Research: Space Physics, 2014, 119, 4841-4859.	2.4	21
41	Comparison of rotational temperature derived from groundâ€based OH airglow observations with TIMED/SABER to evaluate the Einstein coefficients. Journal of Geophysical Research: Space Physics, 2015, 120, 10069-10082.	2.4	20
42	Global structure and seasonal variations of the migrating 6-h tide observed by SABER/TIMED. Science China Earth Sciences, 2015, 58, 1216-1227.	5.2	20
43	Multiday thermospheric density oscillations associated with variations in solar radiation and geomagnetic activity. Journal of Geophysical Research: Space Physics, 2015, 120, 3829-3846.	2.4	20
44	Longitudinal Thin Structure of Equatorial Plasma Depletions Coincidently Observed by <i>Swarm</i> Constellation and all‣ky Imager. Journal of Geophysical Research: Space Physics, 2018, 123, 1593-1602.	2.4	20
45	Clobal distributions of OH and O2 (1.27 μm) nightglow emissions observed by TIMED satellite. Science China Technological Sciences, 2011, 54, 447-456.	4.0	19
46	Longitudinal variations of nighttime electron auroral precipitation in both the Northern and Southern hemispheres from the TIMED global ultraviolet imager. Journal of Geophysical Research, 2011, 116, .	3.3	18
47	Annual asymmetry in thermospheric density: Observations and simulations. Journal of Geophysical Research: Space Physics, 2013, 118, 2503-2510.	2.4	18
48	Recent investigation on the coupling between the ionosphere and upper atmosphere. Science China Earth Sciences, 2014, 57, 1995-2012.	5.2	18
49	Thermospheric planetary waveâ€ŧype oscillations observed by FPIs over Xinglong and Millstone Hill. Journal of Geophysical Research: Space Physics, 2014, 119, 6891-6901.	2.4	18
50	Alfvén waves as a solar-interplanetary driver of the thermospheric disturbances. Scientific Reports, 2016, 6, 18895.	3.3	18
51	Spectral analysis of ionospheric electron density and mesospheric neutral wind diurnal nonmigrating tides observed by COSMIC and TIMED satellites. Geophysical Research Letters, 2009, 36, .	4.0	17
52	The emission of oxygen green line and density of O atom determined by using ISUAL and SABER measurements. Annales Geophysicae, 2012, 30, 695-701.	1.6	17
53	First U.S.â€China joint groundâ€based Fabryâ€Perot interferometer observations of longitudinal variations in the thermospheric winds. Journal of Geophysical Research: Space Physics, 2014, 119, 5755-5763.	2.4	17
54	Characteristics of mesospheric gravity waves over the southeastern Tibetan Plateau region. Journal of Geophysical Research: Space Physics, 2016, 121, 9204-9221.	2.4	17

#	Article	IF	CITATIONS
55	Equatorial <i>E</i> Region Electric Fields and Sporadic <i>E</i> Layer Responses to the Recovery Phase of the November 2004 Geomagnetic Storm. Journal of Geophysical Research: Space Physics, 2017, 122, 12,517.	2.4	17
56	The responses of the nightglow emissions observed by the TIMED/SABER satellite to solar radiation. Journal of Geophysical Research: Space Physics, 2016, 121, 1627-1642.	2.4	16
57	Evaluation of processes that affect the photochemical timescale of the sodium layer. Journal of Atmospheric and Solar-Terrestrial Physics, 2005, 67, 1216-1225.	1.6	15
58	Estimation of the equivalent Rayleigh friction in mesosphere/lower thermosphere region from the migrating diurnal tides observed by TIMED. Journal of Geophysical Research, 2009, 114, .	3.3	15
59	Doubleâ€layer structure of OH dayglow in the mesosphere. Journal of Geophysical Research: Space Physics, 2015, 120, 5778-5787.	2.4	15
60	A Comparison of Quiet Time Thermospheric Winds Between FPI Observations and Model Calculations. Journal of Geophysical Research: Space Physics, 2018, 123, 7789-7805.	2.4	15
61	Responses of Lower Thermospheric Temperature to the 2013 St. Patrick's Day Geomagnetic Storm. Geophysical Research Letters, 2018, 45, 4656-4664.	4.0	15
62	Strong Gravity Waves Associated With Tonga Volcano Eruption Revealed by SABER Observations. Geophysical Research Letters, 2022, 49, .	4.0	15
63	Seasonal variation of the Hough modes of the diurnal component of ozone heating evaluated from Aura Microwave Limb Sounder observations. Journal of Geophysical Research, 2010, 115, .	3.3	14
64	The first observation of the atmospheric tides in the mesosphere and lower thermosphere over Hainan, China. Science Bulletin, 2010, 55, 1059-1066.	1.7	13
65	Temporal evolution of nightglow emission responses to SSW events observed by TIMED/SABER. Journal of Geophysical Research, 2011, 116, .	3.3	13
66	Gravity Wave Propagation from the Stratosphere into the Mesosphere Studied with Lidar, Meteor Radar, and TIMED/SABER. Atmosphere, 2019, 10, 81.	2.3	13
67	Midlatitudinal Special Airglow Structures Generated by the Interaction Between Propagating Mediumâ€Scale Traveling Ionospheric Disturbance and Nighttime Plasma Density Enhancement at Magnetically Quiet Time. Geophysical Research Letters, 2019, 46, 1158-1167.	4.0	12
68	Observations of the first meteorological rocket of the Meridian Space Weather Monitoring Project. Science Bulletin, 2011, 56, 2131-2137.	1.7	11
69	Fiveâ€day waves in polar stratosphere and mesosphere temperature and mesospheric ice water measured by SOFIE/AIM. Journal of Geophysical Research D: Atmospheres, 2015, 120, 3872-3887.	3.3	11
70	Interaction of Oppositely Traveling Mediumâ€Scale Traveling Ionospheric Disturbances Observed in Low Latitudes During Geomagnetically Quiet Nighttime. Journal of Geophysical Research: Space Physics, 2021, 126, e2020JA028723.	2.4	11
71	Global balanced wind derived from SABER temperature and pressure observations and its validations. Earth System Science Data, 2021, 13, 5643-5661.	9.9	11
72	Studies of gravity wave–induced fluctuations of the sodium layer using linear and nonlinear models. Journal of Geophysical Research, 2004, 109, .	3.3	10

#	Article	IF	CITATIONS
73	Terannual variation in the <i>F</i> ₂ layer peak electron density (<i>N</i> _{<i>m</i>} <i>F</i> ₂) at middle latitudes. Journal of Geophysical Research, 2012, 117, .	3.3	10
74	Simulations of large winds and wind shears induced by gravity wave breaking in the mesosphere and lower thermosphere (MLT) region. Annales Geophysicae, 2014, 32, 543-552.	1.6	10
75	Statistical study of atmospheric gravity waves in the mesopause region observed by a lidar chain in eastern China. Journal of Geophysical Research D: Atmospheres, 2015, 120, 7619-7634.	3.3	10
76	Evolution processes of a group of equatorial plasma bubble (EPBs) simultaneously observed by groundâ€based and satellite measurements in the equatorial region of China. Journal of Geophysical Research: Space Physics, 2017, 122, 4819-4836.	2.4	10
77	Edge Plasma Enhancements of Equatorial Plasma Depletions Observed by Allâ€6ky Imager and the C/NOFS Satellite. Journal of Geophysical Research: Space Physics, 2018, 123, 8835-8849.	2.4	10
78	On the Sources of the Ionospheric Variability in the South American Magnetic Anomaly During Solar Minimum. Journal of Geophysical Research: Space Physics, 2019, 124, 7638-7653.	2.4	10
79	Equatorial plasma bubbles developing around sunrise observed by an all-sky imager and global navigation satellite system network during storm time. Annales Geophysicae, 2020, 38, 163-177.	1.6	10
80	Different Sporadic‣ (Es) Layer Types Development During the August 2018 Geomagnetic Storm: Evidence of Auroral Type (Es _a) Over the SAMA Region. Journal of Geophysical Research: Space Physics, 2022, 127, .	2.4	10
81	Solar activity dependency of multiday oscillations in the nighttime thermospheric winds observed by Fabryâ€Perot interferometer. Journal of Geophysical Research: Space Physics, 2015, 120, 5871-5881.	2.4	9
82	Persistent longitudinal variations in 8 years of CIPS/AIM polar mesospheric clouds. Journal of Geophysical Research D: Atmospheres, 2016, 121, 8390-8409.	3.3	9
83	Evolution of a Mesospheric Bore in a Duct Observed by Groundâ€Based Doubleâ€Layer Imagers and Satellite Observations Over the Tibetan Plateau Region. Journal of Geophysical Research: Space Physics, 2019, 124, 1377-1388.	2.4	9
84	New Findings Relating Tidal Variability and Solar Activity in the Low Latitude MLT Region. Journal of Geophysical Research: Space Physics, 2022, 127, .	2.4	9
85	Automatic Extraction of Gravity Waves from All-Sky Airglow Image Based on Machine Learning. Remote Sensing, 2019, 11, 1516.	4.0	8
86	Observing System Impact on Ionospheric Specification Over China Using EnKF Assimilation. Space Weather, 2020, 18, e2020SW002527.	3.7	8
87	First Look at a Geomagnetic Storm With Santa Maria Digisonde Data: <i>F</i> Region Responses and Comparisons Over the American Sector. Journal of Geophysical Research: Space Physics, 2021, 126, e2020JA028663.	2.4	8
88	First experiment of spectrometric observation of hydroxyl emission and rotational temperature in the mesopause in China. Science China Technological Sciences, 2012, 55, 1312-1318.	4.0	7
89	The responses of ionospheric topside diffusive fluxes to two geomagnetic storms in October 2002. Journal of Geophysical Research: Space Physics, 2014, 119, 6806-6820.	2.4	7
90	The Seasonal and Longitudinal Variations of Nighttime OI 135.6â€nm Emission at Equatorial Ionization Anomaly Crests Observed by the DMSP/SSUSI. Journal of Geophysical Research: Space Physics, 2020, 125, e2019JA027764.	2.4	7

#	Article	IF	CITATIONS
91	Interaction Between a Southwestward Propagating MSTID and a Poleward Moving WSA‣ike Plasma Patch on a Magnetically Quiet Night at Midlatitude China Region. Journal of Geophysical Research: Space Physics, 2020, 125, e2020JA028085.	2.4	7
92	Nocturnal and Seasonal Variation of Na and K Layers Simultaneously Observed in the MLT Region at 23°S. Journal of Geophysical Research: Space Physics, 2020, 125, e2019JA027164.	2.4	7
93	The Influence of Ionospheric Neutral Wind Variations on the Morphology and Propagation of Medium Scale Traveling Ionospheric Disturbances on 8th August 2016. Journal of Geophysical Research: Space Physics, 2021, 126, e2020JA029037.	2.4	7
94	Statistics of gravity wave spectra in the troposphere and lower stratosphere over Beijing. Science China Earth Sciences, 2010, 53, 141-149.	5.2	6
95	Influences of non-isothermal atmospheric backgrounds on variations of gravity wave parameters. Science China Technological Sciences, 2012, 55, 1251-1257.	4.0	6
96	Characteristics and mechanisms of the annual asymmetry of thermospheric mass density. Science China Earth Sciences, 2015, 58, 540-550.	5.2	6
97	Strong temperature gradients and vertical wind shear on MLT region associated to instability source at 23A°S. Journal of Geophysical Research: Space Physics, 2017, 122, 4500-4511.	2.4	6
98	First OH Airglow Observation of Mesospheric Gravity Waves Over European Russia Region. Journal of Geophysical Research: Space Physics, 2018, 123, 2168-2180.	2.4	6
99	A Case Study of the Stratospheric and Mesospheric Concentric Gravity Waves Excited by Thunderstorm in Northern China. Atmosphere, 2018, 9, 489.	2.3	6
100	Interaction Between an EMSTID and an EPB in the EIA Crest Region Over China. Journal of Geophysical Research: Space Physics, 2021, 126, e2020JA029005.	2.4	6
101	Occurrence characteristics of branching structures in equatorial plasma bubbles: a statistical study based on all-sky imagers in China. Earth and Planetary Physics, 2021, 5, 407-415.	1.1	6
102	Ionospheric Plasma Vertical Drift and Zonal Wind Variations Cause Unusual Evolution of EPBs During a Geomagnetically Quiet Night. Journal of Geophysical Research: Space Physics, 2021, 126, e2021JA029893.	2.4	6
103	Comparison of horizontal velocity spectra derived from chaff rockets with saturation models. Journal of Geophysical Research, 2006, 111, .	3.3	5
104	The heating efficiency of the exothermic reaction HÂ+ÂO ₃ in the mesosphere. Journal of Geophysical Research D: Atmospheres, 2015, 120, 12739-12747.	3.3	5
105	Lidar observation campaigns on diurnal variations of the sodium layer in Beijing and Wuhan, China. Science China Earth Sciences, 2015, 58, 1377-1386.	5.2	5
106	Comparison of Thermospheric Winds Measured by GOCE and Groundâ€Based FPIs at Low and Middle Latitudes. Journal of Geophysical Research: Space Physics, 2021, 126, e2020JA028182.	2.4	5
107	Gravity-wave-perturbed wind shears derived from SABER temperature observations. Atmospheric Chemistry and Physics, 2020, 20, 14437-14456.	4.9	5
108	Performance of the IRI-2016 over Santa Maria, a Brazilian low-latitude station located in the central region of the South American Magnetic Anomaly (SAMA). Annales Geophysicae, 2020, 38, 457-466.	1.6	5

#	Article	IF	CITATIONS
109	The gravity wave instability induced by photochemistry in summer polar mesopause region. Science Bulletin, 2000, 45, 267-272.	1.7	4
110	Diurnal variations of turbulence parameters over the tropical oceanic upper troposphere during SCSMEX. Science China Technological Sciences, 2014, 57, 351-359.	4.0	4
111	Possible modulation of migrating diurnal tide by latitudinal gradient of zonal wind observed by SABER/TIMED. Science China Earth Sciences, 2016, 59, 408-417.	5.2	4
112	Responses of Multiday Oscillations in the Nighttime Thermospheric Temperature to Solar and Geomagnetic Activities Measured by Fabryâ€Perot Interferometer in China. Journal of Geophysical Research: Space Physics, 2019, 124, 9420-9429.	2.4	4
113	Characteristics of Highâ€Energy Proton Responses to Geomagnetic Activities in the Inner Radiation Belt Observed by the RBSP Satellite. Journal of Geophysical Research: Space Physics, 2019, 124, 7581-7591.	2.4	4
114	Statistical Structure of Nighttime O ₂ Aurora From SABER and Its Dependence on Geomagnetic and Solar Activities in Winter. Journal of Geophysical Research: Space Physics, 2020, 125, e2020JA028302.	2.4	4
115	AÂcomparison of OH nightglow volume emission rates as measured by SCIAMACHY and SABER. Atmospheric Measurement Techniques, 2020, 13, 3033-3042.	3.1	4
116	Main Wave Sources of the Longitudinal Structures of Equatorial Electric Field. Geophysical Research Letters, 2021, 48, e2021GL092426.	4.0	4
117	Global static stability and its relation to gravity waves in the middle atmosphere. Earth and Planetary Physics, 2020, 4, 1-9.	1.1	4
118	Gravity wave activity in the troposphere and lower stratosphere: An observational study of seasonal and interannual variations. Journal of Geophysical Research D: Atmospheres, 2013, 118, 11,352.	3.3	3
119	Nighttime anomaly of ionospheric electron density. Science China Earth Sciences, 2016, 59, 1517-1518.	5.2	3
120	Effects of solar proton events on dayglow observed by the TIMED/SABER satellite. Journal of Geophysical Research: Space Physics, 2017, 122, 7619-7635.	2.4	3
121	Persistent Layers of Enhanced Gravity Wave Dissipation in the Upper Mesosphere Revealed From SABER Observations. Geophysical Research Letters, 2022, 49, .	4.0	3
122	Daytime lidar measurements of the sodium layer in China. Science China Earth Sciences, 2016, 59, 1707-1708.	5.2	2
123	The study and applications of photochemical-dynamical gravity wave model I. Science in China Series A: Mathematics, 2002, 45, 167-174.	0.5	1
124	Characteristics of low altitude ionospheric electric field over Hainan Island, China. Science China Earth Sciences, 2017, 60, 770-775.	5.2	1
125	Extraction of Quasi-Monochromatic Gravity Waves from an Airglow Imager Network. Atmosphere, 2020, 11, 615.	2.3	1
126	Simultaneous Observation of Sporadic Potassium and Sodium Layers Over São José dos Campos, Brazil (23.1°S, 45.9°W). Journal of Geophysical Research: Space Physics, 2021, 126, e2020JA028890.	2.4	1

#	Article	IF	CITATIONS
127	Upwelling coherent backscatter plumes observed with ionosondes in low-latitude region. Journal of Space Weather and Space Climate, 2022, 12, 13.	3.3	1
128	Effects of gravity waves on the distributions of O3 and OH in the mesopause region. Science Bulletin, 2001, 46, 1265-1268.	1.7	0
129	The criterion of gravity wave instability induced by photochemistry in summer polar mesopause region. Science in China Series D: Earth Sciences, 2002, 45, 512-520.	0.9	0
130	The study and applications of photochemical-dynamical gravity wave model II. Science in China Series A: Mathematics, 2002, 45, 175-182.	0.5	0
131	Linear theory of the response of Na mixing ratio to gravity waves. Science Bulletin, 2003, 48, 1630-1633.	1.7	0
132	Study on the Distribution of the Sodium Layer over Wuhan, China Based on the Lidar Observations. Chinese Journal of Geophysics, 2003, 46, 823-833.	0.2	0
133	Cause of winter gravity wave spectrum saturation. Science in China Series D: Earth Sciences, 2005, 48, 1802-1808.	0.9	0
134	Nonlinear interactions between gravity waves and tides. Science in China Series D: Earth Sciences, 2007, 50, 1273-1279.	0.9	0
135	Determination of Methane Cracking in Pyrolysis Experiment and its Geochemical Significance. , 2021, , .		0
136	Lidar Observations in South America. Part I - Mesosphere and Stratosphere. , 0, , .		0